We are IntechOpen, the world's leading publisher of Open Access books Built by scientists, for scientists

4,800
Open access books available

122,000
International authors and editors

135M
Downloads

Our authors are among the

154
Countries delivered to

TOP 1%
most cited scientists

12.2%
Contributors from top 500 universities

WEB OF SCIENCE™

Selection of our books indexed in the Book Citation Index in Web of Science™ Core Collection (BKCI)

Interested in publishing with us?
Contact book.department@intechopen.com

Numbers displayed above are based on latest data collected.
For more information visit www.intechopen.com

Chapter 6

Flow Accelerated Corrosion in Nuclear Power Plants

Wael H. Ahmed

Additional information is available at the end of the chapter

http://dx.doi.org/10.5772/51346

1. Introduction

In general, corrosion is defined as the degradation of a material by means of chemical reactions with the surrounding environment. Several types of corrosion occur in a variety of situations in the nuclear power plants. Some of these types are common such as rusting of steel when located in moist environment, and the other type of corrosion such as flow accelerated corrosion required special treatment due to their impact on the plant safety and reliability. FAC degradation mechanism results in thinning of large areas of piping and fittings that can lead to sudden and sometimes to catastrophic failures, as well as a huge economic loss. FAC is a process caused by the flowing water or wet steam damaging or thinning the protective oxide layer of piping components. The FAC process can be described by two mechanisms: the first mechanism is the soluble iron production (Fe2+) at the oxide/water interface, while the second mechanism is the transfer of the corrosion products to the bulk flow across the diffusion boundary layer. Although the FAC is characterize by a general reduction in the pipe wall thickness for a given piping component, it frequently occurs over a limited area within this component due to the local high area of turbulence. The rate of the metal wall loss due to FAC depends on a complex interaction of several parameters such as material composition, water chemistry, and hydrodynamic.

In general, erosion processes or mechanisms can be categorized as:

i. **Shear stress erosion**: In this category, the surface of a material gets destroyed in single-phase flow at high velocity, by the effects of shear stresses and the variations in the fluid velocity.
ii. **Liquid impact induced erosion**: This form of erosion occurs in two-phase flow by the impingement of liquid droplets entrained in flowing gases or vapours. It can cause damages to power plant condenser tubes, elbows, turbine blades, etc. The wear process

can however be avoided by a combination of improvements in: plant design, drying the steam, and the use of more corrosion-resistant steels.

iii. **Flashing-induced erosion:** This form of erosion occurs when spontaneous vapour formation takes place due to sudden pressure changes. Locations where this type of erosion occurs are found in drain and vent lines downstream of control valves.

iv. **Cavitation erosion:** This type of erosion is caused by repeated growth and collapse of bubbles in a flowing fluid as a result of local pressure fluctuations. In the regions of higher pressures downstream, the sudden collapse of gas bubbles results in pressure spikes that may erode the material in their vicinity. These bubbles will however get re-absorbed along the piping system without causing any damage to the downstream straight piping component.

On the other hand, degradation mechanisms involve combined effect of chemical and mechanical processes can be summarized as:

i. **Erosion-corrosion: In this mechanism** a combination of mechanical and chemical material degradation processes take place. The combined effect of the two processes is considered more severe especially in the case when copper alloy heat exchanger tubes are exposed to high velocities.

ii. **Flow-Accelerated Corrosion:** The pipe wall thinning due to this degradation mechanism in carbon steel piping is not due to the mechanical effect only, however, the wall thinning is mainly due to dissolution of normally protective magnetite film that normally forms on the internal pipe wall surface.

1.1. Conditions required for FAC

It has been observed that the following conditions result in FAC degradation in nuclear or fossil power plants:

- Flow conditions: both single- and two-phase flow conditions, with water or water-steam mixture as the flowing liquid, at a temperature of > 95^{o}C, and flow velocity is greater than zero.
- Chemistry condition: the flowing liquid should be such that a potential difference exists between the liquid and the carbon steel pipe wall. This difference will be responsible for the dissolution of the protective oxide layer in the flowing stream. A high magnetite solubility and subsequent rapid removal of the magnetite, is facilitated by either demineralised and neutral water or slightly alkalinized water under reducing conditions.
- Material: the pipe material must be carbon steel or low-alloy steel. General practice recommends that for a well-designed system, FAC will be effectively inhibited if steel components are made to contain at least 0.1% chromium.
- Flow Geometry: FAC has been observed to occur downstream of flow-restricting or redirecting geometries like an orifice, sudden contraction, expansion, elbows, reducers, etc.

Failures and accidents due to FAC degradation have been reported at several nuclear power plants around the world since 1981 [1]. However, detailed analysis of the FAC related

failures did not start before the severe elbow rapture downstream of a tee occurred at Surry Unit 2 power plant (USA) in 1989, which caused four fatalities and extensive plant damage and resulted in a plant shutdown. In 1999, an extensive steam leakage from the rupture of the shell side of a feed-water heater at the Point Beach power plant (USA) was reported by Yurmanov and Rakhmanov [2] (Figure 1). In 2004, a fatal pipe rupture downstream of an orifice in the condensate system due to FAC occurred in the Mihama nuclear power plant Unit 3 (Japan) [2]. More recently, the pipe failure downstream of a control valve at Iatan fossil power plant in 2007 resulted in two fatalities and a huge capital of plant loss as reported by Moore [3]. Although, a combination of lab research and attempts to correlate lab results with plant experience has been the major efforts made towards the study of FAC mechanism since the 1970's, the lab research only focused on understanding the mechanisms, and correlating experimental results in order to reduce the lab effort and to develop usable forms for the plant engineers. Several well cited correlations used to predict the actual corrosion rates due to FAC in piping systems and incorporated in computer software such as CHECWORKS developed by Electric Power Research Institute (EPRI). Following the abovementioned accidents, most utilities around the world have been following EPRI guideline of improving the flow water chemistry to slow down the rate of damage. Also, in the event of disposition of highly susceptible or damaged areas, utilities have typically taken the following initial steps:

1. Replace individual worn components with other components of same material.
2. Replace individual worn components with other components of FAC resistant material.
3. Replace entire worn lines with other components of same material.
4. Replace entire susceptible lines or the more susceptible portions with other components of FAC resistant material.

The recent review by Ahmed [4] highlighted the significant research conducted on investigating the effect of fluid chemical properties on flow accelerated corrosion (FAC) in nuclear power plants. He concluded that the hydrodynamic effects of single and two-phase flows on FAC have not been thoroughly investigated for many piping components. In order to determine the effect of the proximity between two components on the FAC wear rate, Ahmed [4] has investigated 211 inspection data for 90^{o} carbon steel elbows from several nuclear power plants. The effect of the velocity as well as the distance between the elbows and the upstream components was discussed. Based on the analyzed trends obtained from the inspection data, the author indicated a significant increase in the wear rate of approximately 70% that was identified to be due to the proximity.

Furthermore, the repeated inspections in nuclear power plants have shown that piping components located downstream of flow singularities, such as sudden expansion or contractions, orifices, valves, tees and elbows are most susceptible to FAC damage. This is due to the severe changes in flow direction as well as the development of secondary flow instabilities downstream of these singularities [4]. Moreover, in two-phase flows, the significant phase redistributions downstream of these singularities may aggravate the problem. Therefore, it is important to identify the main flow and geometrical parameters

require in characterizing FAC damage downstream of pipe fittings. These parameters are: the geometrical configuration of the components, piping orientation, and the flow turbulence structure which will affect the surface shear stress and mass transfer coefficients.

18” elbow wall thickness decreased from 12.7 to 1.5 mm on feed-water pump inlet at Surry, 1986

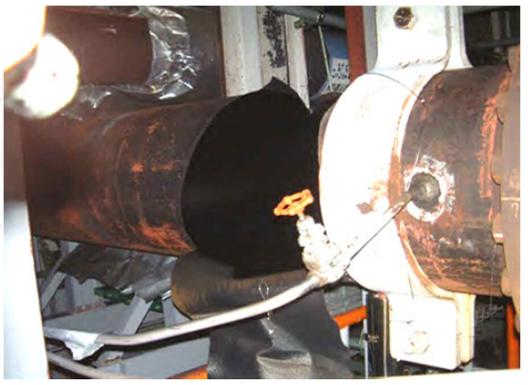

Wall Thickness reduced from 10 to 1.5 mm on Feed-water piping at Mihama unit 3, 2004

Failure in a high pressure extraction line at Fort Calhoun in 1997

Failure downstream of the LCV in the reheater drain line at Millstone unit 2, 1991.

Failure of 14” heater drain extraction line to high pressure heater at Arkansas unit 2, 1986

Failure of the Feed-water Heater Point Beach Unit 1, 1999

Figure 1. Examples of failures due to FAC worldwide (Yurmanov and Rakhmanov [2])

For single phase flow, the secondary vortices and/or flow separation downstream of pipe fittings considered to be important parameters need to be analyzed and modelled while predicting the highest FAC wear rate location. For example; the secondary flows in elbows induce a pressure drop along the elbow wall that can significantly increase the wall mean and oscillatory shear stresses as discussed by Crawford et al. [5]. Also, orifices and valves promote turbulence close to the wall in the downstream pipe and thus enhance the rate of mass transfer at the wall [5]. These mechanisms have been identified as the governing factors responsible for FAC as explained by Chen et al. [6].

The hydrodynamics parameters controlling FAC in two-phase flows are considered more complex than for single-phase flows due to the complexity of two-phase distribution and the unknown interactions between the gas phase and the liquid [8]. These interactions play a major role in the mass, momentum, and energy transfer between the flow phases as explained by Hassan et al. [9]. Also, the inlet two-phase flow pattern plays an important role in the flow dynamics downstream of the orifices since the phase redistribution downstream depend on the upstream flow regime. For example, bubbles can have significant effects on the turbulent kinetic energy close to the wall, affecting the wall shear stress and pressure. Moreover, Jepson [10] showed that high velocity slugs can cause high turbulence and shear forces at the pipe wall and thus enhance the destruction of the protective inhibitor film.

Computational fluid dynamic (CFD) analysis is used to predict turbulent fluid flow with great accuracy for many applications. However, only the recent advances in computational power have allowed the use of CFD for mass transfer and corrosion studies. This indicated that the accurate prediction of mass transfer near the wall requires resolving the mass transfer boundary layer which may be an order of magnitude smaller than the viscous sub-layer. In order to perform the CFD calculations with good accuracy, fine near-wall grids with correct near-wall turbulence models can therefore provide mass transfer data for the corrosion species. In these cases corrosion is controlled by the mass transfer, relation between the wall mass transfer coefficient and corrosion rate can be derived as explained in details by Keating and Nesic [11]. Furthermore, in formulating the CFD codes, consideration is made to the hydrodynamic parameters affecting the mass transfer rate of the corrosion products to the bulk fluid and consequently the FAC rate. These hydrodynamic parameters are the flow velocity, pipe roughness, piping geometry, and steam quality or void fraction for two-phase flow.

The hydrodynamic effects of the working fluid on FAC have been investigated by many researchers using CFD. Bozzini [12] adopted numerical simulations for investigating wall erosion/corrosion inside a pipe bend for a four-phase flow that comprised of two immiscible liquids, gas and particulate solids. On the other hand, Chang et al. [13] suggested an evaluation scheme to estimate the load carrying capacity of thinned-wall pipes exhibiting FAC. In their study, they employed a steady-state incompressible flow CFD code to determine the pressure distributions as input conditions for a structural finite element

analyses in order to calculate local stresses. More recently, Ferng [14] developed an approach that used an erosion/corrosion model and three-dimensional single and two-phase flow models to predict locations of serious FAC in power plant piping systems. Their predictions agreed very well with plant measurements.

2. FAC rate and mass transfer

The FAC process in carbon steel piping is described by three steps. In the first process, metal oxidation occurs at metal/oxide interface in oxygen-free water and explained by the following reactions:

$$Fe + 2H_2O \rightarrow Fe^{2+} + 2OH^- + H_2 \tag{1}$$

$$Fe^{2+} + 2OH^- \leftrightarrow Fe\left(OH\right)_2 \tag{2}$$

$$3Fe \ + \ 4H_2O \ \rightarrow Fe_3O_4 + \ 4H_2 \tag{3}$$

The first process involves the solubility of the ferrous species through the porous oxide layer into the main water flow. This transport across the oxide layer is controlled by the concentration diffusion. The second step is described by the dissolution of magnetite at oxide/water interface as explained by the following reaction:

$$1/3Fe_3O_4 + \left(2-b\right)H^+ + 1/3H_2 \leftrightarrow Fe\left(OH\right)_b^{(2-b)+} + \ \left(4/3-b\right)H2O) \tag{4}$$

where:

$Fe(OH)_b^{(2-b)+}$ represents the different iron ferrous species $b=(0,1,2,3)$

In the third step (Eq. 4), a diffusion process takes place where the ferrous irons transfer into the bulk flowing water across the diffusion boundary layer. In this process, the species migrated from the metal/oxide interface and the species dissolved at the oxide/water interface diffuse rapidly into the flowing water. In this case, the concentration of ferrous iron in the bulk water is very low compared to the concentration at the oxide/water interface.

It can be noticed that FAC mechanism involves convective mass transfer of the ferrous ions in the water. The convective mass transfer for single phase flow is known to be dependent on the hydrodynamic parameters near the wall interface such as flow velocity, local turbulence, geometry, and surface roughness. In addition, the physical properties of the transported species or the water do not affect the local transport rate in adiabatic flow especially when temperature changes in piping system are negligible. Over a limited length of piping component, FAC rate is considered as direct function of the mass flux of ferrous ions and can be calculated from the convective mass transfer coefficient (*MTC*) in the flowing water. Then, FAC rate is calculated from the MTC and the difference between the concentration of ferrous ions at the oxide/water interface (C_w) and the concentration of ferrous in the bulk of water (C_b) as:

$$FAC\ rate\ =\ MTC(\ C_w\ -\ C_b) \tag{5}$$

Several research works [15-17] showed that MTC is one of the important parameters affecting FAC and the experimental data are often expressed in terms of Sherwood (*Sh*), Reynolds (*Re*) and Schmidt (*Sc*) numbers as:

$$Sh\ =\ a.Re^b.Sc^c \tag{6}$$

where *a*, *b* and *c* are related to mass transfer which occurs under a given flow condition and can only be obtained experimentally. Where (*Sh)* in the non-dimensional representation of MTC as a function of the local hydrodynamic parameters and expressed as:

$$Sh\ =\ MTC.d_H\ /\ D \tag{7}$$

where: d_H = hydraulic diameter, and *D* = diffusion coefficient of iron in water.

In Equation (6), the velocity exponent varies between 0.8 for lower Reynolds numbers and 1.0 for very high Reynolds numbers. This difference in the velocity exponent is caused by the surface roughness. This indicates that the FAC rate increases as the surface roughness increases. It should be also noted that the experimental studies and the correlations developed for MTC were carried out under low flow rates conditions compared with common operating conditions in power generation industry. Therefore, the MTC data obtained in the literature for moderate and high Reynolds numbers at power plant conditions can lead to significant errors.

In the case of piping downstream orifices, Tagg et al. [18] described the wear enhancement profile empirically in terms of the maximum Sherwood number using Reynolds number at the vena contracta section (Re_o) as follows:

$$Sh_{max} = 0.27 \cdot Re_o^{0.67} \cdot Sc^{0.33} \tag{8}$$

On the other hand, the local enhancement profile downstream of the orifice at different axial locations (z) is described empirically by Coney [19] referred to by Chexal et al. [20] as:

$$\frac{Sh_z}{Sh_{fd}} = 1 + A_Z\left[1 + B_Z\left(\frac{Re_o^{0.66}}{0.0165 \cdot Re^{0.86}} - 21\right)\right] \tag{9}$$

where Sh_{fd} is the Sherwood number for the smooth straight pipe, Sh_z is the Sherwood number at any axial location (z), A_z and B_z are empirical constants.

Another modelling approach for FAC prediction was carried by Remy et al., [21], to develop a criteria in order to avoid FAC damage. They model the FAC mechanism as a combination of two main mechanisms. These mechanisms are divided into two steps. In the first of which is the production of soluble ferrous ions, which is represented by a first-order reaction:

$$V_C\ =\ \mathrm{K}\ (\mathrm{C_{eq}}\text{- C}) \tag{10}$$

V_C = total corrosion rate, K = reaction rate constant, C_{eq} = the soluble ion concentration at oxide water interface. The second step of FAC is correlated to the transfer of ferrous ion into the bulk water, which is a convective transport phenomenon that can be modelled as:

$$F_{IF} = k (C - C_{\infty}) \tag{11}$$

where: F_{IF} = the ferrous ion flux, MTC = mass transfer coefficient, C_{∞} = ferrous ion concentration in the bulk flow. These two steps are assumed to be equal at equilibrium state, and can be expressed in terms of the combined equation:

$$V_C = 2K(MTC) (C_{eq} - C)/(MTC + 2K) \tag{12}$$

which was finally reduced to:

$$T_L = kC_{eq} \tag{13}$$

T_L is the thickness loss kinetic which is mainly correlated to the FAC wear rate. This conclusion of linear relationship between FAC rate and concentration was early refuted by Poulson [22], giving reasons in favour of non-linearity. These reasons including:

a. removal of a surface film above a critical value of K, e.g. carbon steel in nitrate solutions,
b. interactions of anodic and cathodic areas, e.g. iron in Nacl or $FeCl_3$ solutions,
c. coupling of reactions, where flow effects K, which changes the corrosion potential and also the oxide solubility (ΔC). This leads to a dependency on K^n (where n is between 1 and 3), and
d. dual control, e.g. situations in which the rate is partially controlled by activation such as copper alloys in seawater, or alternatively by two transport processes. This tends to lead to a dependency on K^n, where n is less than 1.

A comprehensive report on FAC in power plants, by EPRI [3], presents empirical models that have been used successfully to predict components that are most likely to wear, and provide reasonable estimates of pipe wall-thinning. These models are however computer-based due to the large amount of information that needs to be processed. These models are represented in the following two groups:

i. Berge model

The model assumed that the chemical dissolution of the magnetite at the oxide/water interface occurs in accordance with the following equation:

$$DR = K (C_{eq} - C_S) \tag{14}$$

where DR is the ferrous iron production rate; K is the reaction rate constants or (kinetics); Ceq, is the equilibrium concentration of magnetite; and C_S, is the magnetite concentration at oxide/water interface. Finally, the FAC rate is given as:

$$FAC \text{ rate } = 2K (C_{eq} - C_S) \tag{15}$$

ii. MIT model

This model is mainly an improved version of Berge's model considering the diffusion through the porous oxide layer and incorporating both oxide thickness (δ) and porosity (Θ), and also considers diffusion of iron hydroxides through the pores, to determine the FAC rate as:

$$FAC \text{ rate } = \frac{\theta(C_{eq} - C_{\infty})}{\left(1/K^{*} + (1-f)(1/k + \delta/D)\right)} \tag{16}$$

3. FAC modelling in two-phase flow

For FAC under two-phase flow condition, Remy et al. [21] indicated that same correlations used for single-phase flow calculations are also applicable in two-phase flow calculations. The only difference in the analysis is the calculation of actual Reynolds number, using the actual water velocity taking into account the void fraction between the steam and water.

EPRI report [3] incorporated the idea of Remy et al. [21] on the use of single phase correlations in clculating FAC under two-phase flow conditions. Calculation begin by determining Reynolds number for the liquid phase, Re_L, as follows:

$$\mathrm{Re}_L = V_L \frac{d_H}{\upsilon_L} \tag{17}$$

Where the liquid velocity expressed as:

$$V_L = \left(\frac{Q}{A\rho_L}\right).\left(\frac{1-x}{1-\alpha}\right) \tag{18}$$

The flow is considered to be a single phase liquid flow when the steam quality (x) and the steam void fraction (α) are both equal to zero (0), while $\alpha = 1$ implies no presence of liquid, hence $Re_L = 0$ and no FAC damage is expected. Under two-phase flow conditions, when (α) is greater than (x), and $Re_L > Re$, the mass transfer coefficient increases and consequently FAC wear rate increases.

In two-phase flow the void fraction is usually not equal to steam quality because the liquid and the vapour phases are moving with different velocities, and sometimes in different directions. If homogeneous flow is assumed, the two phase's velocities are assumed to be equal, which results in a steam quality-void fraction relationship as a function of pressure. However, due to the fact that the homogeneous flow assumption is not suitable for many industrial applications, more sophisticated models were developed by researchers to relate steam quality to void fraction. One of the most cited model is the Chexal-Lellouche void model:

$$\langle \alpha \rangle = \frac{\langle j_g \rangle}{C_O \langle j \rangle + \overline{V_{gj}}} \tag{19}$$

where:

$\langle j \rangle$ and $\langle j_g \rangle$ are the mixture and vapour volumetric fluxes.

Another model developed by Kuo-Tong et al. [23] to predict FAC damage locations on High pressure (HP) turbine exhaust steam line. Their choice of High pressure (HP) turbine exhaust steam line as a case study was based on the plant measured data of pipe thickness which indicated HP lines as a good example where serious FAC takes place under two phase flow conditions. They reported that FAC phenomenon strongly depends on the piping layout and local flow conditions. They proposed a new mathematical approach to simulate FAC wear rate. The approach includes the use of 3D two-phase flow hydrodynamic CFD model to simulate the two-phase flow behaviour in HP lines, integrated with FAC Models to investigate the impact of the local parameters on FAC damage. The improvement of their new approach over the previous work is the ability to account for the multi-dimensional characteristics applied to FAC wear rate prediction. This is consider a great advantage in predicting FAC compared to the previous codes such as CHECKWORK or CAECE program which are based on empirical correlations that are dependent on the global flow conditions in the piping lines. In developing their code, the following assumptions were adopted:

- Adiabatic flow, since the piping in the type of the above-cited facilities is generally thermally insulated.
- Droplet-type two-phase flow, because of the high steam quality (> 85%) usually experienced in the studied piping. Hence, the vapour phase (steam) was modelled as a continuous phase and the liquid droplet as a dispersed phase.
- Simplified geometries, where valves in the piping are not considered.

Their final hydrodynamic CFD models include two-fluid 3D continuity and momentum equations. Closure relations such as the mixture *k-e* turbulent models, two-phase constitutive equations were also used. The developed FAC model claimed to include droplet impingement model, which was used to simulate the mechanically-assisted form of material degradation.

In a similar two-phase flow analysis applied to the extraction piping system connecting the low-pressure turbine (LPTB) and feed water heater (FWH) at boiling water reactors (BWR), Yuh et al. [24] developed a code to predict FAC wear in BWR piping system. Their mathematical approach is very similar to the work done by Kuo-Tong et al. [23], with the exception to the addition of corrosion model used. They obtained the local distributions of fluid parameters including two-phase flow velocities, void fractions, turbulent properties, and pressure. These results were further used to establish the relation for droplet kinetic energy that represents the FAC damage. The comparison of between their model and the plant measured data show qualitatively a good agreement.

4. FAC prediction downstream an orifice

Once the relationship between mass transfer and FAC wear rate is established, the computational model for MTC downstream of an orifice can be formulated. Fully developed

turbulent pipe flow is assumed in order to determine MTC profiles downstream of the orifice. ANSI specifications of orifice were used to construct the geometrical model. Since the experimental condition in the present study is carried out for straight pipe section fabricated from hydrocal (CaSO4.½H2O) downstream of an orifice to simulate faster effect of mass transfer rates. The Solution is obtained for Renormalization Group (RNG) *K-ℰ* differential viscosity model for turbulent flow in conjunction with the species transport equations using FLUENT CFD code.

The velocity field of the incompressible viscous flow is obtained using the one dimensional Reynolds averaged governing equations as follows:

Continuity equation:

$$\frac{\partial \bar{u}_i}{\partial x_i} = 0 \left(\frac{\partial \mathrm{u}_\mathrm{i}'}{\partial \mathrm{x}_\mathrm{i}} = 0 \right) \tag{20}$$

Momentum equation:

$$\bar{u}_j \frac{\partial \bar{u}_i}{\partial x_j} = -\frac{\partial \bar{P}}{\partial x_i} + \frac{\partial}{\partial x_j}\left(\frac{1}{\mathrm{Re}} \frac{\partial \bar{u}_i}{\partial x_j} - \overline{u_i' u_j'} \right) \tag{21}$$

Species mass transport equation for a steady process with no chemical reaction is:

$$\nabla.(\rho \vec{v} Y_i) = -\nabla.\vec{J}_i + S_i \tag{22}$$

where: $\vec{J}_i$ is the diffusion flux of species *i,* and arises due to concentration gradient, and S_i is the source term.

In Equation (11), the Boussinesq eddy viscosity assumption [25] is used for modeling the Reynold's stress. The eddy viscosity model relation is expressed as:

$$-\rho \overline{u_i u_j} = \mu_t[(\partial U_i / \partial z_j) + (\partial U_j \partial z_i)] - 2\rho k \delta_{ij} / 3 \tag{23}$$

where μ_t is defined as the "turbulent viscosity" and expressed as:

$$\mu_t = C_\mu f_\mu (\rho k^2 / \varepsilon) \tag{24}$$

The turbulence kinetic energy (k) and the turbulence kinetic energy dissipation rate (ε) are defined as follows:

$$k = (\overline{u^2} + \overline{v^2} + \overline{w^2})/2, \ \varepsilon = v\overline{(\partial u_i / \partial z_j)^2} \tag{25}$$

Therefore, the equation for turbulence kinetic energy can be also expressed as follows:

$$\frac{\partial(\rho U k)}{\partial z} + (1/r)\frac{\partial(r\rho V k)}{\partial r} = \frac{\partial[(\mu_{eff} / \sigma_k)(\partial k / \partial z)}{\partial z} + [1/r]\frac{\partial[(r\mu_{eff} / \sigma_k)(\partial k / \partial r)]}{\partial r} + G_k - \rho\varepsilon \tag{26}$$

and the equation for the turbulence kinetic energy dissipation expressed as:

$$\frac{\partial(\rho U\varepsilon)}{\partial z}+(1/r)\frac{\partial(r\rho V\varepsilon)}{\partial r}=\frac{\partial[(\mu_{eff}/\sigma_{\varepsilon})(\partial\varepsilon/\partial z)}{\partial z}+[1/r]\frac{\partial[(r\mu_{eff}/\sigma_{\varepsilon})(\partial\varepsilon/\partial r)]}{\partial r}+ \\ (\varepsilon/k)(C_{\varepsilon 1}f_1G_k-C_{\varepsilon 2}f_2\rho\varepsilon) \tag{27}$$

In Equations (16) and (17) the generation of kinetic energy of turbulence term (G_k) can be written as:

$$G_k=\mu_{eff}[2[(\partial U/\partial z)^2+(\partial V/\partial r)^2+(V/r)^2]+[(\partial U/\partial r)+(\partial V/\partial z)]^2] \tag{28}$$

where the effective viscosity (μ_{eff}) is defined as:

$$\underbrace{\mu_{eff}}_{effective}=\underbrace{\mu}_{molecular}+\underbrace{\mu_t}_{turbulent} \tag{29}$$

The calculation of the local MTC is obtained similar to El-Gammal et al. [26] as:

$$MTC(z)=\frac{-D_{SL}\partial c/\partial n|_w}{(c_w-c_b)} \tag{30}$$

where c_w is the species concentration along the wall (obtained from hydrocal properties table), c_b is the species concentration in the bulk flow beyond the diffusive boundary layer, n is the normal vector to the wall surface and D_{SL} is the diffusive coefficient of the solid species, which is calculated by using Wilkie's semi-empirical relationship, [26]:

$$D_{SL}=\frac{7.4\times10^{-15}\times T\times\sqrt{\Psi\times M_S}}{\eta\times V^{0.6}} \tag{31}$$

where T is the temperature (K), Ψ is the association factor for the solvent (2.6 for water), M_S is the molecular mass for the solvent (18 g for water), η is the solvent absolute viscosity (Pa.s), V is the molecular volume of the dissolved species (144.86cm^3/mol for hydrocal) at ambient temperature.

The concentration of hydrocal species in the bulk of water c_b is calculated as follows:

$$c_b(z)=\frac{1}{\rho UA}\int\rho u(r)c(r)dA \tag{32}$$

where U is the area average velocity, $u(r)$ is the instantaneous flow velocity, $c(r)$ is the species concentration profile, and A is the cross sectional area of the pipe. The term $\partial c/\partial n|_w$ (z) is calculated by taking the concentration gradient at the wall at an axial location (z). Substituting equations (31) and (32) into equation (30), the cross-sectional average for $MTC(z)$ along the axial direction can be calculated.

In order to evaluate the FAC wear rate downstream orifice, the conservation equations are integrated over each control volume in the flow field which extended upstream downstream of the orifice. Reynolds Average Navier-Stokes equations were solved using the K-Ɛ (RNG) differential viscosity turbulence model to account for low-Reynolds-number (LRN) effects. The solution convergence is greatly improved by using fine near-wall grids. Also, the computational mesh was refined where high velocity and species concentration gradients were expected. Due to the high Schmidt numbers encountered in mass transfer problems, Nesic et al. [27] suggested that the maximum value of Y^+ should not exceed 0.1.The Reynolds average mass transport equation was also solved for determining the concentration field of the dissolved wall species.

For the present case study, numerical simulations were performed at Reynolds number, *Re* = 20,000 and orifice-to-pipe diameter ratios of *d*/*D* = 0.25, 0.5 and 0.74. Prior to the commencement of the simulations, a sensitivity study of three different grid numbers was performed and the results indicate a deviation in flow characteristics within ±2%. The flow characteristics for the three orifice geometries are found to be qualitatively similar. Therefore, only representative vector and contour plots for *d*/*D* = 0.5 are presented here. Fig. (2a) shows the mean velocity vectors normalized by the averaged inlet velocity (U_O) within

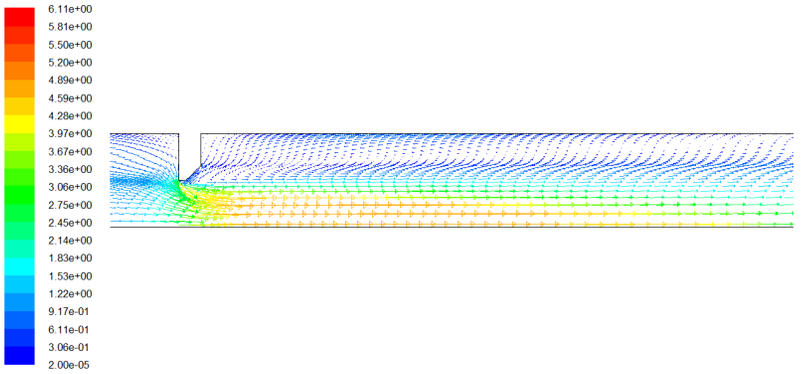

a) Normalized mean velocity vectors downstream the orifice

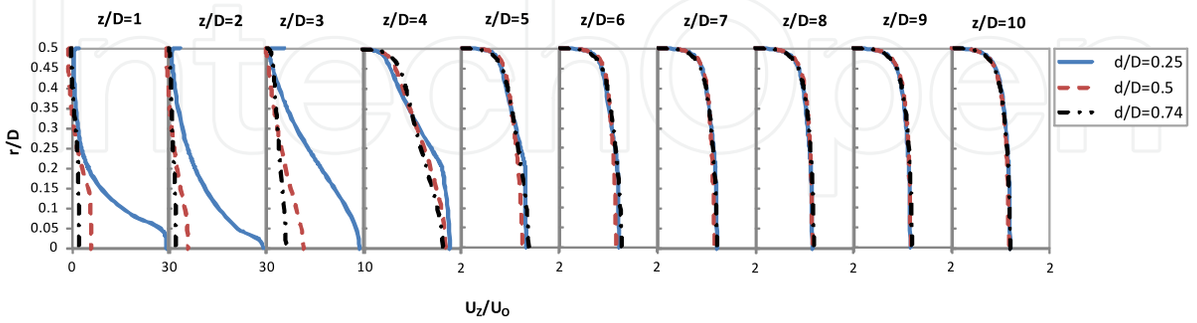

b) Profiles of normalized horizontal velocity component (*Re* = 20,000 d/D = 0.25, 0.5 and 0.74)

Figure 2. Numerical results for the flow downstream orifice

the flow domain. It can be seen that the flow accelerates as it approaches the orifice then separates at the sharp edges of the orifice, forming large vortices downstream. These

vortices sustain the reduction in the flow cross-sectional area further downstream up to the minimum area known as the vena contracta, after which the flow decelerates towards the flow reattachment point. This is the cause of the high velocity central region observed just downstream the orifice which changes to lower velocity region as the flow develops further downstream. Fig. (2b) shows the profiles of the mean horizontal velocity for the three geometries at different axial locations. The ordinate r/D is measured from the centreline of the pipe while Z/D is measured from the orifice. As shown in the figure, the maximum centreline velocity increases within the circulation zone as the orifice diameter decreases. The relative reductions in the centreline velocity at Z/D=1 through Z/D=4 are about 93%, 92%, 75% and 5.7% respectively, as d/D increases from 0.25 to 0.74. Downstream Z/D = 5, the velocity profiles are almost similar for the three geometries, with the flow returning to fully developed turbulent flow at $Z/D \cong 30$. The flow reattachment length downstream the orifice also increases as the orifice diameter decreases, with the shortest at $Z/D \cong 2$ for $d/D = 0.74$, or by $Z/D \cong 3$ for $d/D = 0.5$ and $Z/D \cong 4$ for $d/D = 0.25$.

Another important flow parameter that can be related to the FAC is the skin friction coefficient C_f which is defined as $C_f = \tau_w/(1/2\rho U_o^2)$, where τ_w is the wall shear stress. The distribution of C_f downstream the orifice for the three d/D ratios are illustrated in Fig. (3). Variation of C_f is found to be similar for the three d/D ratios. Typical profile show an increase steeply downstream the orifice due to the reversed flow generated by the separating vortices, and reaches a maximum value at $Z/D \cong 0.4$, 1.3 and 2.3, for $d/D = 0.74$,

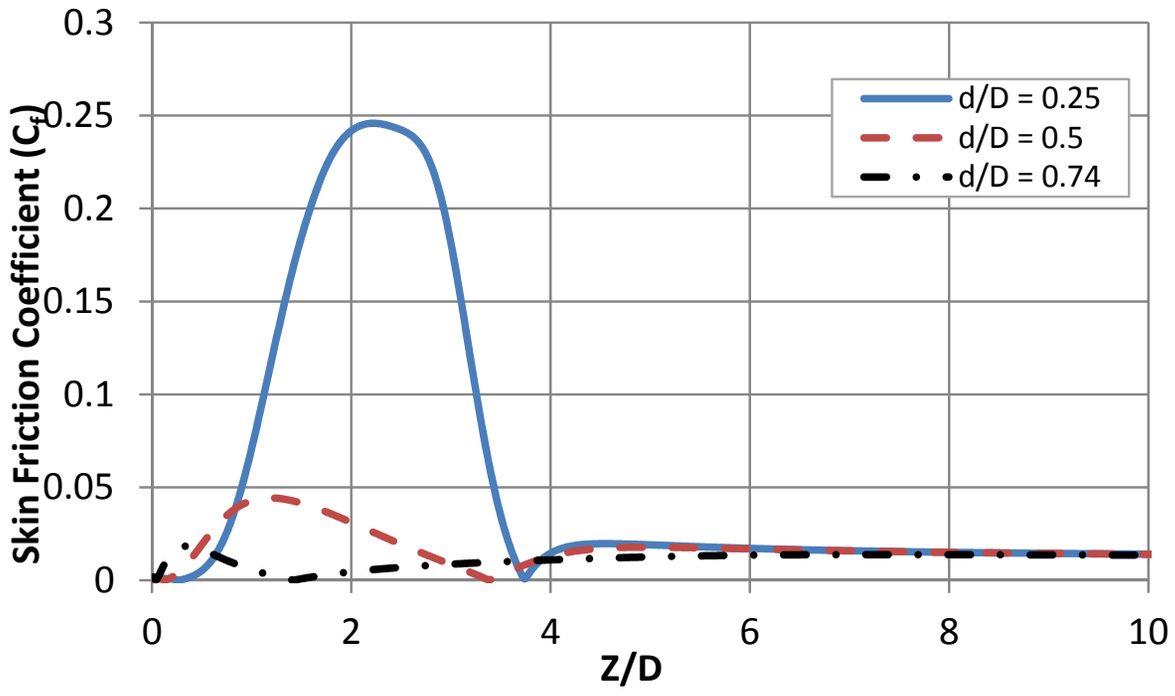

Figure 3. Skin friction coefficient along the pipe wall downstream the orifice for different orifice diameters

0.5 and 0.25 respectively. The skin friction coefficient then decreases steeply and reaches a minimum value at $Z/D \cong 1.4$, 3.4 and 3.7, for d/D = 0.74, 0.5 and 0.25 respectively, within the flow re-attachment region. As the flow progresses downstream, the surface shear stress increases due to the boundary layer developed by the reattached flow, and reaches the second local peak between Z/D = 4 and 5. These local peak values of C_f decrease as d/D increases, the first value decreases by about 92% as d/D increases from 0.25 to 0.74, while the second value decreases marginally. In general, the shear stress found to decrease as the boundary layer thickness increases downstream restricting orifices.

The contours of normalized turbulent kinetic energy (*TKE)* within the flow domain for d/D = 0.5 are shown in Fig. (4a). *TKE* increases appreciably within the flow separation zone due to the high velocity gradients within this region. Fig. (4b) shows the profiles of the normalized

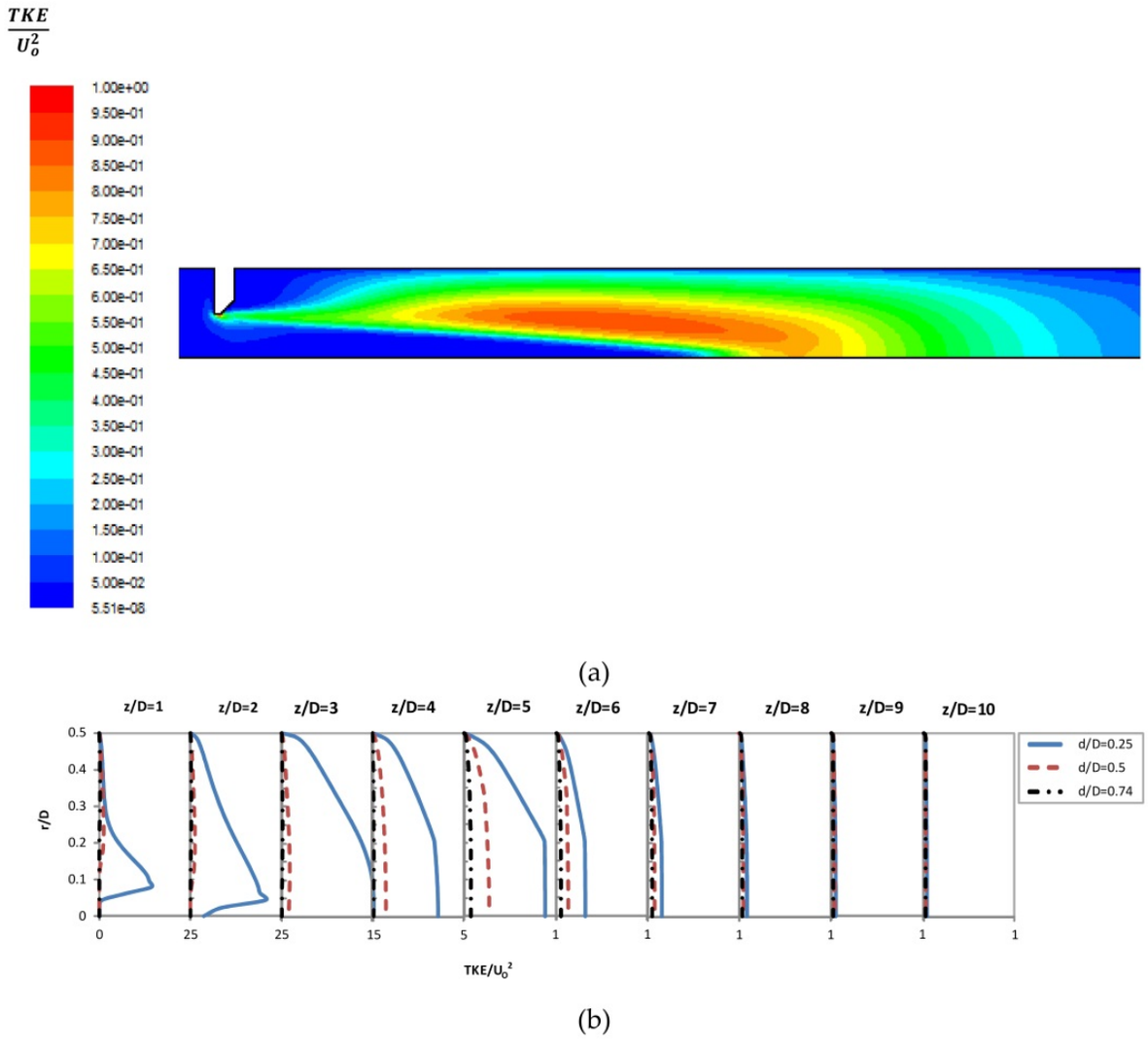

Figure 4. (a) – Contours of normalized turbulent kinetic energy downstream the orifice, for d/D = 0.5 and *Re* = 20,000 and (b) radial profiles of normalized turbulent kinetic energy at *Re* = 20,000.

TKE for the three d/D at different axial locations downstream the orifice. The profiles are found to be qualitatively similar for all the three d/D; within the circulation region (Z/D = 0 –

2). The normalized *TKE* value increases from zero at the wall to a maximum value at the centreline. These local peak values of *TKE*, as well as its radial location from the wall, increase as *d*/*D* decreases. All the profiles however collapse to a single line at *Z*/*D* = 8 as the flow becomes fully developed. The axial distribution of normalized *TKE* downstream the orifice is shown in Fig. (4b) for the three *d*/*D* ratios. Moreover, the peak value of *TKE* decreases by about 96% as *d*/*D* increases from 0.25 to 0.74.

The predicted *MTC* distributions downstream the orifice is shown in Fig. (5). The mass transfer found to increase sharply downstream the orifice and reaches a peak value at *Z*/*D* ≅ 1, 4 and 3, for *d*/*D* = 0.74, 0.5 and 0.25 respectively, after which it decreases steeply to the fully developed value downstream. The *MTC* distributions found to correlate very well with the *TKE* profiles. The non-dimensional mass transfer coefficient represented by Sherwood number (*Sh)* and the mass transfer enhancement Sh_zSh_{fd} downstream the orifice are shown in Figs. (6a and 6b). The peak value of *Sh*, as well as Sh_zSh_{fd}, decreases by about 63% and 42% when *d*/*D* increases from 0.25 to 0.5 and from 0.5 to 0.74 respectively. The axial locations of the peak values however move downstream from *Z*/*D* ≅ 1 to 4 when *d*/*D* decreases from 0.74 to 0.5, while the peak locations move upstream from *Z*/*D* ≅ 4 to 3 when *d*/*D* decreases from 0.5 to 0.25.

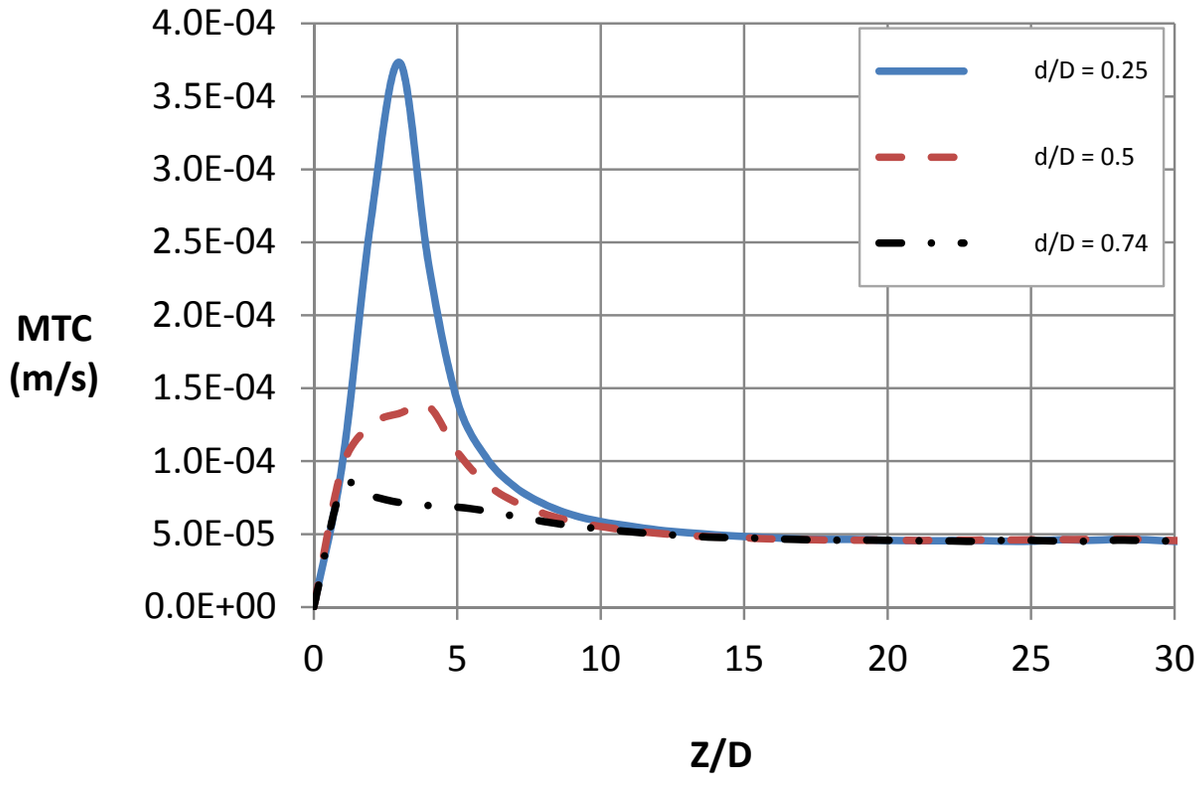

Figure 5. Mass transfer coefficient distributions downstream the orifice (*Re* = 20,000)

FAC rate downstream the orifice is shown in Fig. (7) for different *d*/*D* ratios. The peak value of *FAC* increases as *d*/*D* decreases. In the present analysis, the peak value increases by about 90% when *d*/*D* decreases from 0.74 to 0.25. Moreover, the axial locations of the peak values however

move downstream from $Z/D \cong 1$ to 3 as d/D decreases from 0.74 to 0.25. The location of *FAC* peak values found to also correlate very well with the location of the peak *TKE*.

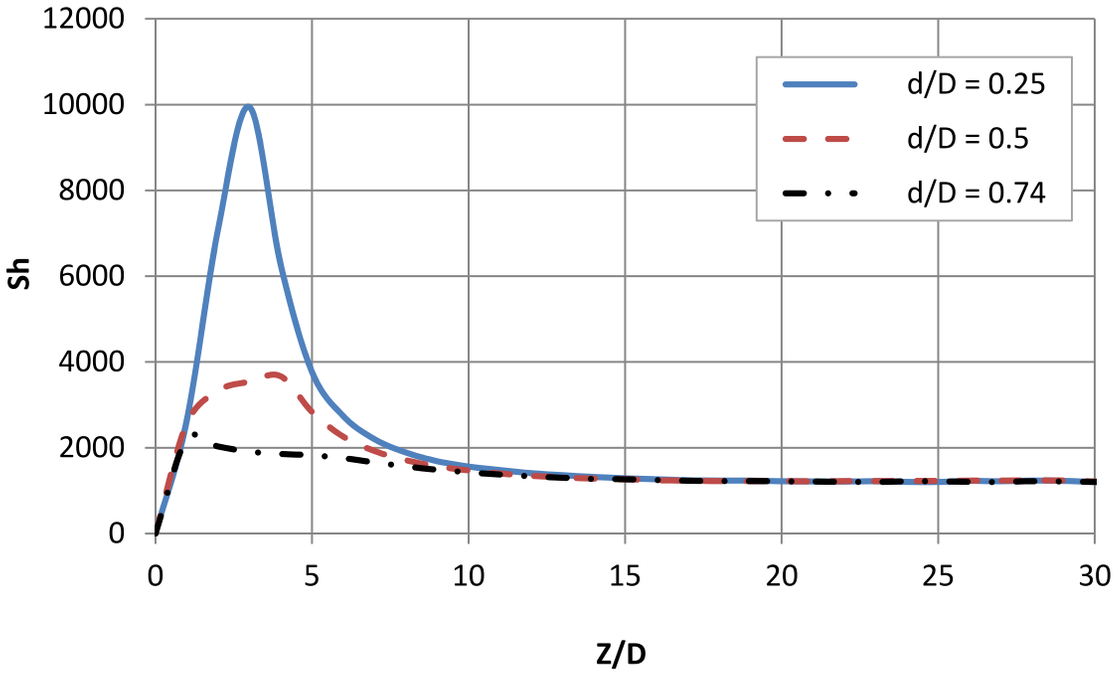

a

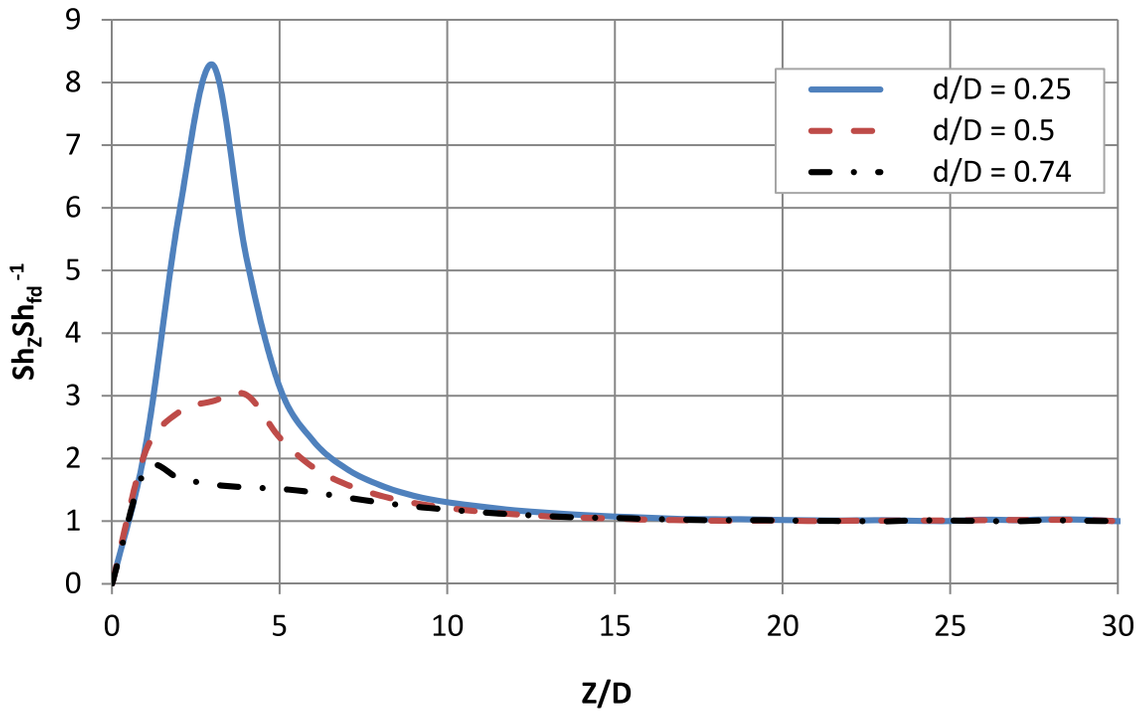

Figure 6. a: Sherwood number distributions downstream the orifice, for different orifice diameters, and *Re* = 20,000, b: Enhancement of mass transfer downstream the orifice, for different orifice diameters, and Re = 20,000

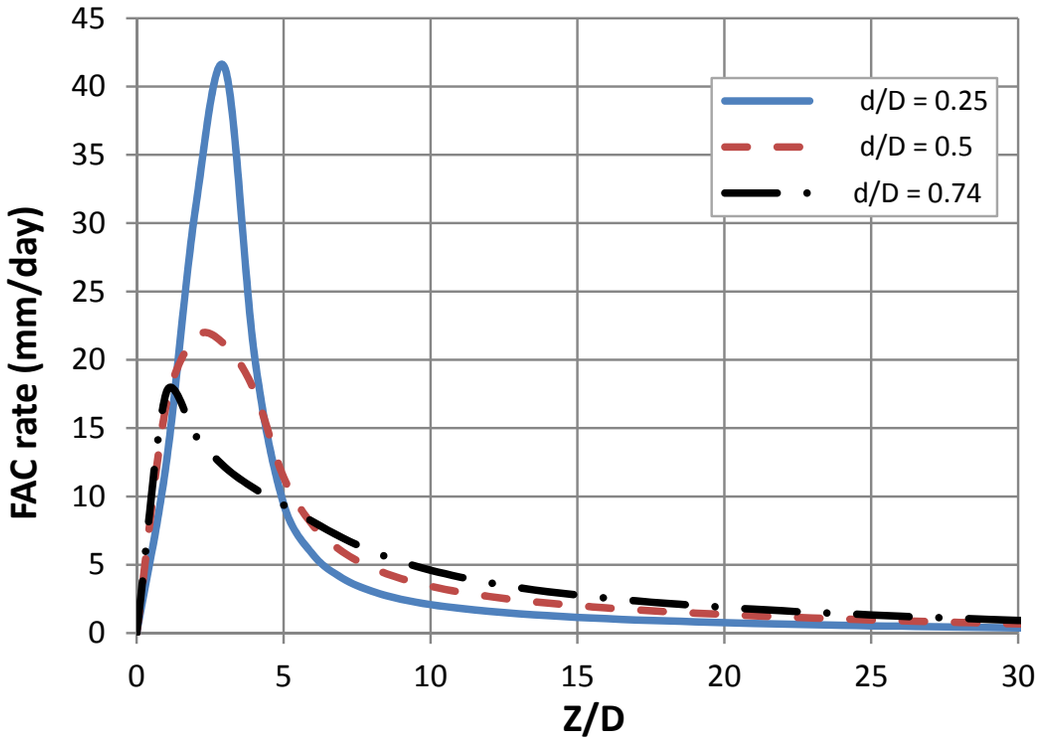

Figure 7. FAC wear rate downstream the orifice, for different orifice diameters, and $Re = 20{,}000$

4.1. Power plants inspection data

Ultrasonic techniques (UT) measurements are commonly used to determine the wall thinning measurement in nearly all power plants and to provide more accurate data for measuring the remaining wall thickness in piping system. The UT inspection data were obtained at grid intersection points marked on the piping component. The data are usually stored in a data logger and transferred to a PC for further processing using appropriate software. The wall thickness data were obtained at different grid point on the piping as shown in Fig. (8). For each pipe downstream an orifice, the difference between the measured wall thickness and the nominal pipe wall thickness is calculated and considered to be the wear at this axial location along the pipe. Sometimes, scanning within grids and recording the minimum found within each grid square is an acceptable alternative to the above method. However, it should also be noted that scanning within grids and the minimum wall thickness recorded can affect the accuracy of the data if point-to-point comparison between two consecutive inspections times. The inspection data are used to determine whether the component has experienced wear and to identify the location of maximum wall thinning as well as to evaluate the wear rate and indentify wear pattern in piping component.

In the present case study, 132 inspection data collected from 5 nuclear power plants and 3 fossil power plants for piping downstream an orifice were analyzed. The data of very high and low values of wear are compared to adjacent inspection readings in order to remove data outliers. Once the data set for each inspection location is verified, the wear is identified at each band along the pipe axis. The measured wear data at different location from the orifice were presented for different piping systems as shown in Fig. (9). It can be concluded

that the effect of geometry found to strongly affect the FAC wear rate downstream of the orifice. The maximum value of the wear found to be located within 5D downstream of the orifice which agrees very well with the inspection data collected from different power plants. Also, the hydrodynamic profiles such as *TKE* and *MTC* found to characterize the FAC wear rate downstream the orifice and the value of the maximum FAC wear rate increases as the orifices diameter reduces.

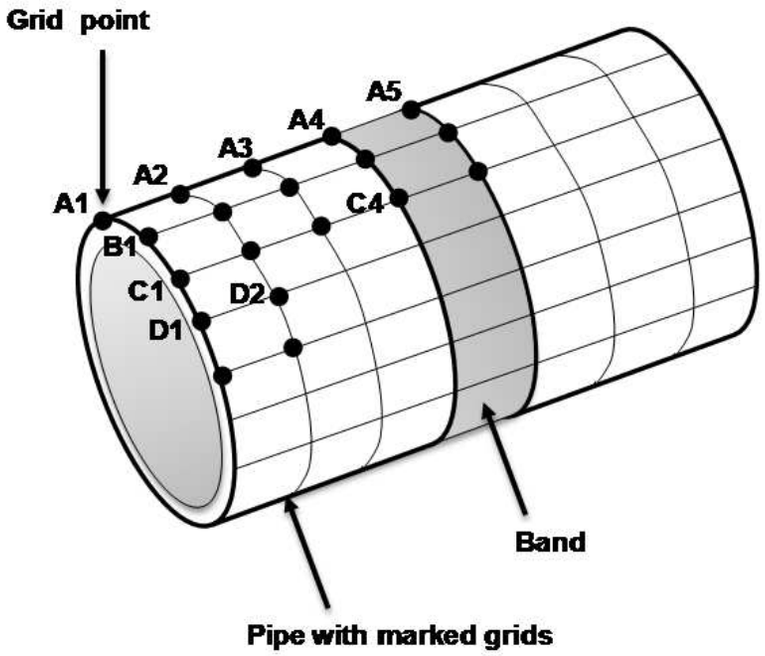

Figure 8. Inspection grids downstream of the orifice

5. Effect of proximity between piping components on FAC

From the above case study of the flow downstream an orifice, it can be concluded that the size and the geometry of a piping component directly influence the flow velocity and hence the local mass transfer rate. In addition, components with geometries that promote increase in the velocity and turbulence tend to experience higher FAC rate such as elbow, tee, reducers and valves, etc. The effect of turbulence on the FAC rate is represented by the geometry enhancement factor as described by Chexal et al. [20]. Moreover, a component that has another component located close upstream experience more turbulence that further increases the FAC rate. One would expect that such components tend to experience more severe FAC as discussed by Kastner et al. [28] and Poulson [29]. In fact, the piping geometry at the point of rupture at Surry 2, where the elbow located downstream of a T-fittings, is a strong evidence of the proximity effect.

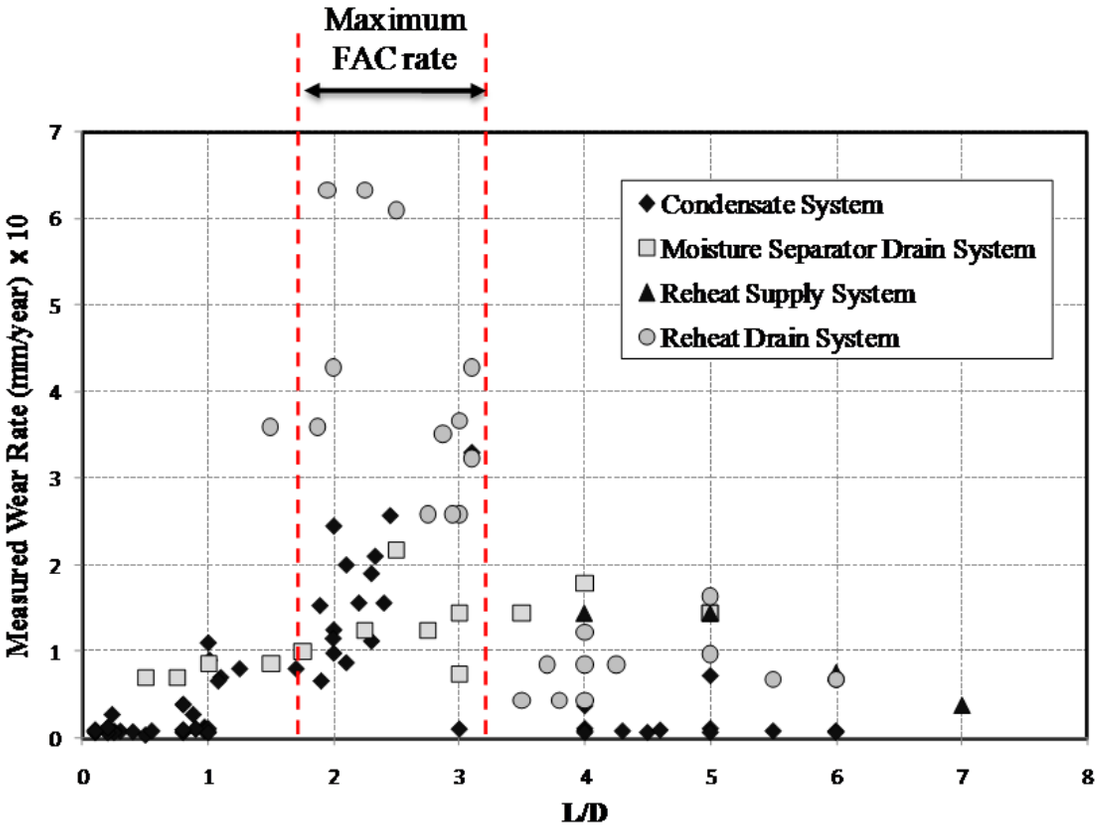

Figure 9. Measured wear rate downstream orifces at different power plants

In summary, a significant amount of research has been conducted on investigating the effect of fluid chemical properties on FAC in nuclear power plants, online monitoring for strategic FAC locations, and FAC control based on chemical fluid decomposition. However, the hydrodynamic effects of single- and two-phase flows on FAC have not been thoroughly investigated, and are currently not well understood. The present case study aims to evaluate the effect of components located in proximity to another component upstream on the pipe wall-thinning rate due to FAC using real inspection data from different degraded elbows in several power plants. Also, to inspire future discussions among the scientific community to revisit the effect of component geometry on FAC wear rate in order establish new codes/correlations that meet actual industrial findings. In order to accomplish this goal, ultrasonic (UT) inspection data for 90° carbon steel elbows for different systems across different nuclear power stations are analyzed in order to quantify the effect of the proximity between components on the FAC wear rate. The effect of the flow velocity as well as the distance between the elbows and the upstream components is also discussed in the present analysis.

The increase in the wear rate due to the proximity is calculated for 90° elbows located within 1D of the upstream Components. Ahmed [4] evaluated several UT data of back-to-back elbows for deferent nuclear power stations as shown in Figure (10). The results are clearly showing an increase in the wear rate due the proximity of the elbow with the upstream components as the majority of the data are consistently above zero. The increase in the wear

rate is approximately equal to 70% in average. The distribution of the data occurrence is plotted in Figure (11) to represent the percentage of components to the total used inspections that have the same wear rate. If a linear wear over the operating time is assumed, one can determine the remaining life of component located in the proximity from another component will results in reduction in component life by more than half life. Although the results show a large scatter of the data with a standard deviation of 50%, the proximity is believed to have a significant effect on the wear rate.

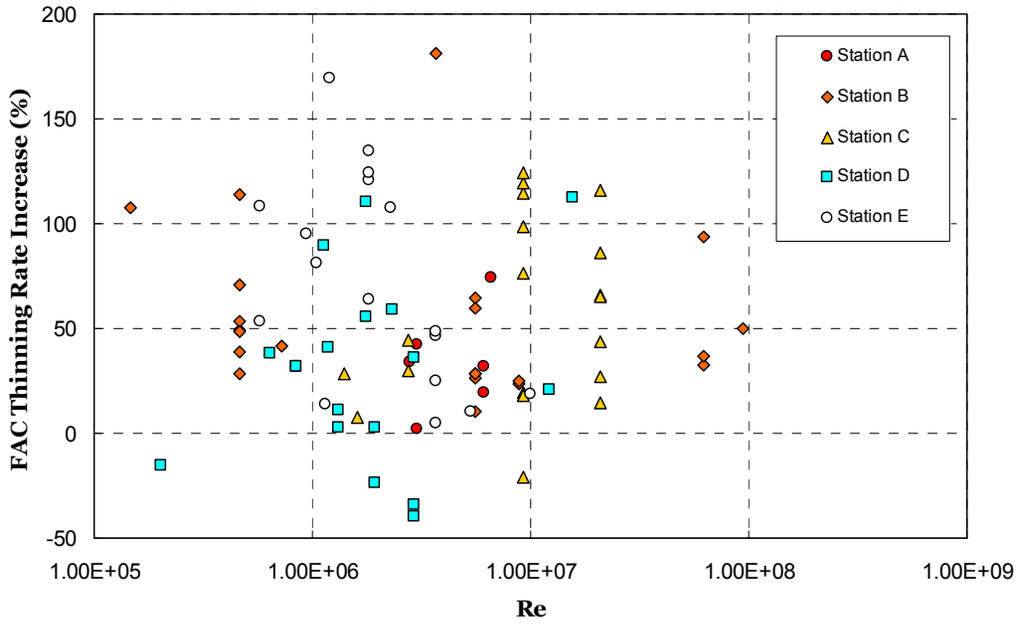

Figure 10. Effect of proximity on FAC wear rate

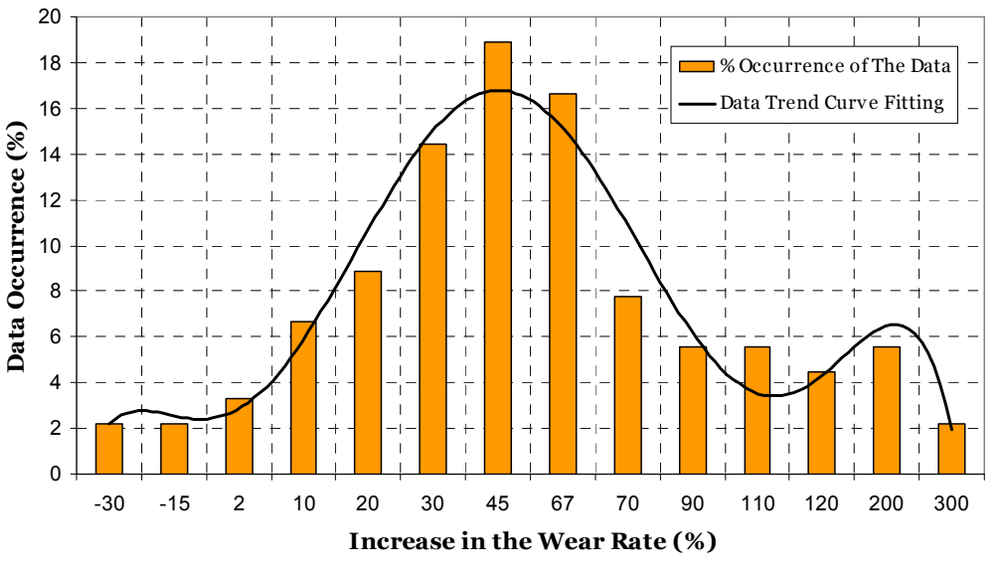

Figure 11. Data occurrence

The other set of UT data is collected for 90° elbows located at different distances (L) from the upstream component are presented. The ratio (L/D) is used to represent the non-dimensional upstream distance with respect to the pipe diameter. As discussed before, a component that has another component located close upstream is expected to experience more turbulence which increases the FAC rate. On the other hand, it is expected that the effect of the turbulence produced from the upstream component becomes much less as the distance from the upstream component increases as shown in Fig. (12). It should be noted that the extent of the proximity effect as shown in Figure (6) is 0 to 5 piping diameters as the a average increase in the wear rate is equal to 70 % (with a standard deviation of 50%) which approximately the same as for elbows within 1D from the upstream components. As the distance between the two components increases the change in the wear rate decreases to reach a minimum value in the fully developed region.

A general trend between the increase in the wear rate and the non-dimensional upstream distance (L/D) is obtained using the average values in the wear rates at different (L/D). The additional effect of the component located upstream close to another component is previously correlated by Kastner et al. (1990) as:

$$\text{Effect of Proximity } (\%) = e^{\left(-0.231 \cdot L/D\right)} \times 100 \tag{33}$$

The average values of FAC wear rate in Fig. (12) are compared to the empirical equation proposed by Kastner et al. [28] and found to be in good agreement with the present data shown in Fig. (13). However, the correlation tends to over predict the data as the distance between the components approaches zero which can be attributed to the accuracy of the proposed correlation and the UT measurements uncertainty.

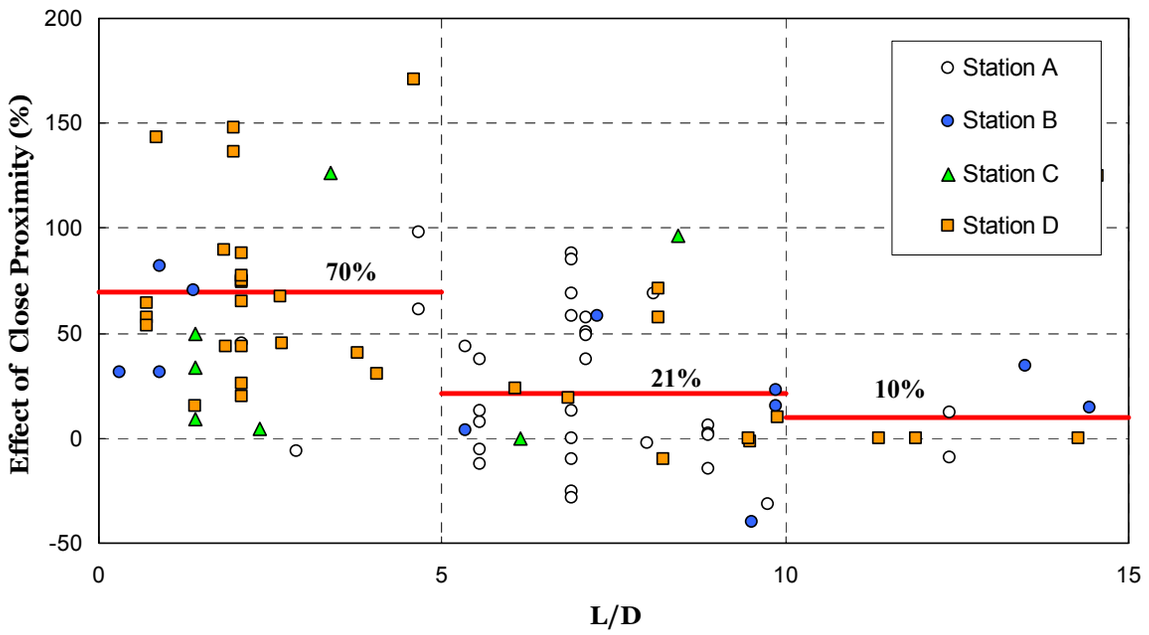

Figure 12. Effect of the upstream distance on the wear rate

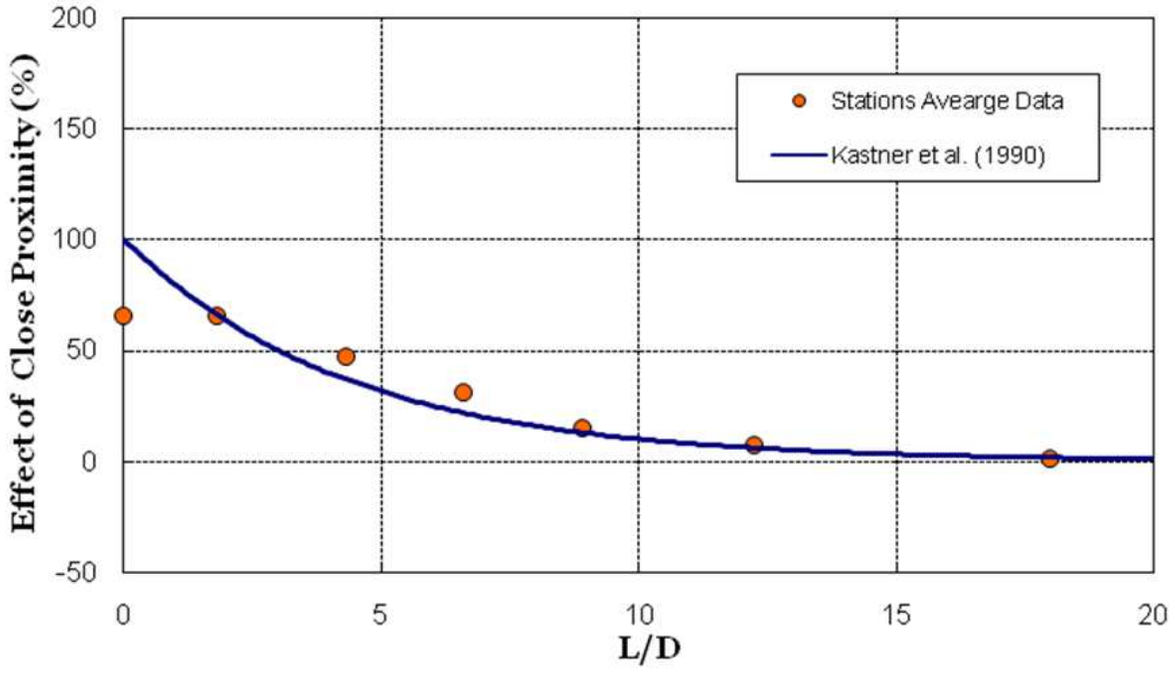

Figure 13. Comparing data with Kastner et al. [28] correlation

As discussed before, components with geometries that promote increase in the flow velocity and turbulence tend to experience higher FAC rate such as elbow, tee, reducers downstream of orifices and valves, etc. Therefore, the turbulence production is expected to be dependent on the component geometry. Consequently, the type of the upstream component could be also considered as a contributing factor and should be considered while performing the flow and mass transfer analysis.

6. Conclusions and recommendations

The effect of geometry found to strongly affect the FAC wear rate. For example, the maximum value of the wear found to be located within 5D downstream of the orifice. Also, the analyzed trends obtained from the plants inspection data show significant increase in the wear rate due to the component proximity. The CFD simulation of the hydrodynamic parameters such as *TKE* and *MTC* found to characterize the FAC wear rate downstream of piping components. Additional experimental and numerical investigations are required to further evaluate the close proximity effect for different components configuration. Findings of the present work will allow the power plant FAC engineers to identify more accurately susceptible components and reduce the inspection scope/time.

Author details

Wael H. Ahmed
Department of Mechanical Engineering, King Fahd University of Petroleum & Minerals, Dhahran, Saudi Arabia

Acknowledgement

The support provided by the Deanship of Scientific Research (DSR) at King Fahd University of Petroleum & Minerals (KFUPM) for funding this research work through project No. IN090038, is gratefully acknowledged. The author also thanks Mr. Mufatiu Bello for carrying out the data analysis of the orifice case study.

Also, the author would like to thank Atomic Energy of Canada Ltd. (AECL), and the CANDU Owner Group (COG) for their support and permission to publish the data on plant close-proximity effect presented in this chapter. The data have been also presented by the author and analyzed in the Annals of Nuclear Energy (37 (2010) 598–605)

7. References

[1] Kanster, W., Erve, M., Henzel, N., and Stellwag, B., (1990), "Calculation code for erosion corrosion induced wall thinning in piping system, Nuclear Engineering and Design, Vol. 119, pp. 431-438.

[2] Yurmanov, V., Rakhmanov, A., (2009), "Workshop on erosion-corrosion, International Atomic Energy Agency, Workshop on Erosion-Corrosion, Moscow, Russian Federation.

[3] Moore, F.E., (2008), "Welding and repair technology for power plants, 18th Int. EPRI Conference.

[4] Ahmed, W.H. (2010), "Evaluation of the proximity effect on flow accelerated corrosion", Annals of Nuclear Energy, Vol. 37, pp. 598-605.

[5] Crawford, N.M., Cunningham, G., Spence, S.W.T. (2007), "An experimental investigation into the pressure drop for turbulent flow in 90° elbow bends" Proc. of the Institution of Mechanical Engineers, Part E, Journal of Process Mechanical Engineering, Vol. 221, no. 2, pp. 77-88.

[6] Poulson B. (1999), "Complexities in predicting erosion corrosion", Wear 233-235, pp. 497-504

[7] Chen X, McLaury B.S., Shirazi S. A.,, (2006), "A Comprehensive Procedure to Estimate Erosion in Elbows for Gas/Liquid/Sand Multiphase Flow " ASME Journal of Energy Resources Technology, Vol. 128, pp. 70-78.

[8] Kim S., Park J.H., Kojasoy G., Kelly J.M., Marshall S.O. (2007), "Geometric effects of 90-degree Elbow in the development of interfacial structures in horizontal bubbly flow ", Nuclear Engineering and Design, Vol.237, 2105-2113

[9] Hassan YA, Schmidl W., Ortiz-Villafuerte J. (1998), "Investigation of three-dimensional two-phase flow structure in a bubbly pipe flow" Measurement Science Technology, Vol. 9, 309-326

[10] Jepson, W. P., (1989), " Modelling the transition to slug flow in horizontal conduit", Canadian Journal of Chemical Engineering, Vol. 67, pp. 731-740

[11] Keating, A., and Nesic, S., (1999), " Prediction of two-phase erosion-corrosion in bends", Second International Conference on CFD in the Mineral and Process Industries, CSIRO, Melbourne, Australia, Dec. 6-8.

[12] Bozzini B., Ricotti M.E., Boniardi M., Mele C. (2003), "Evaluation of erosion-corrosion in multiphase flow via CFD and experimental analysis" Wear, Vol. 255, no. 1-6, pp. 237-245

[13] Chang Y.S., Song K.H., Lee S.M., Choi J.B., Kim Y.J. (2006), Key Engineering Materials, Vol. 321-323, pp. 670-3

[14] Ferng, Y.M., (2008), " Prediction local distribution of erosion-corrosion wear sites for the piping in the nuclear power plant using CFD models" Annals of Nuclear Energy, Vol. 35, no. 2, pp. 304-313.

[15] Poulson B. (1987), "Predicting the occurrence of Erosion-corrosion, Plant corrosion: prediction of material performance, Strutt, J.E., and Nicholls, J. R., Editors, Ellis Horwood Ltd.

[16] Berge, P., and Saint Paul, P., (1981), "Water Chemistry of Nuclear Reactor Systems" Proceedings of the British Nuclear Energy Society, London, P. 19.

[17] Bouchacourt, M., and Remy, F. N., (1991), Proceeding of 3rd NACE international Region Management Committee Symposium, Cambridge, U.K.

[18] Tagg, D. J., Patrick, M. A., and Wragg, A. A., (1979), "Heat and Mass Transfer Downstream of Abrupt Nozzle Expansions in Turbulent Flow "Trans. Inst. Chem. Eng., Vol 57, no 12, pp.176-181.

[19] Coney, M., (1980), CERL Internal Report, Ref: RD/L/N197/80.

[20] Chexal, B., Horowitz, J., Jones, R., Dooley, B., Wood, C., Bouchacourt, M., Remy, F., Nordmann, F., and St. Paul, P., 1996 "Flow-Accelerated Corrosion in Power Plants," Electric Power Research Institute Report No. TR-106611.

[21] Remy, F.N., Bouchacourt, M., 1992, "Flow-assisted corrosion: a method to avoid damage. Nuclear Engineering and Design", 133: p. 23-30.

[22] Poulson, B., 1993,"Advances in understanding hydrodynamic effects on corrosion", Corrosion Science, 35: p. 655-665

[23] Kuo-Tong, M.A., et al. 1998, "Numerically Investigating The Influence Of Local Flow Behaviours On Flow-Accelerated Corrosion Using Two-Fluid Equations", Nuclear Technology, 123: p. 90-102.

[24] Yuh Ming Ferng et al., 2008, "A Two-phase Methodology To Predict FAC Wear Sites In The Piping System of A BWR", Nuclear Engineering and Design, 238: p. 2189-2196.

[25] Boussinesq, J. (1877), "Théorie de l'Écoulement Tourbillant", Mem. Présentés par Divers Savants Acad. Sci. Inst. Fr., Vol. 23, pp. 46-50.

[26] El-Gammal M., Mazhar H., Cotton J.S., Shefski C., Pietralik J., Ching C. Y., (2010), "The hydrodynamic effects of single-phase flow on flow accelerated corrosion in a 90-degree elbow", Nuclear Engineering and Design, vol. 240, 6, pp. 1589-159.

[27] Nesic, S., Adamopoulos, G., Postlethwaite, J. and Bergstrom, D.J.: "Modelling of Turbulent Flow and Mass Transfer with Wall Function and Low-Reynolds Number Closures". The Canadian Journal of Chemical Engineering, Vol. 71, pp. 28-34.

[28] Kastner W., Erve M., Henzel N., and Stellwag B., (1990), Nuc. Eng. Design, v. 119, pp. 431-438.

[29] Poulson, B. (2007), Proc. of 13th Int. Conf. On Environmental Degradation of Materials in Nuclear Power Systems- Canadian Nuclear Soc, Whistler, B.C., Canada.

IntechOpen